Thermal Deformation of Parallelogram Plates under Radiant Heating

Thermal Deformation of Parallelogram Plates under Radiant Heating*

Tsuyoshi SEKIYA**, Seinosuke SUMI**, Eiichi MATSUMOTO,**
Tadakazu KATAYAMA** and Ippei SUGIMOTO***

(Received November 15, 1969)

The deformation of the parallelogram plate clamped along all edges and subjected to uniform radiant heating on one surface was dealt experimentally and theoretically. The temperature rise, the deflection and the strains on the surface of the plate were measured continuously. The thermal buckling phenomenon was observed clearly. The fundamental differential equations for the thermal deformation of the parallelogram plate were solved by the difference method, using the measured temperature distribution and considering the effect of the deformation of the clamping frame. The stress distribution, the critical temperature for buckling and its mode were obtained theoretically and compared with experimental results.

1. Introduction

Not to speak of the sudden temperature rise on the surface of the supersonic aircraft in acceleration, with the remarkable development in various fields of industry, it is becoming more important to appreciate the thermal stresses and deformations in structural elements caused by heating.

Many studies have already been done for the thermoelastic problems of plate which occurred in the field of supersonic aircraft and other industry[1~5]. In Japan, many reports have been published, which dealt with the thermal deformations of plates analytically and experimentally, but those were restricted to the problems of the rectangular plates[6~14].

On the other hand Anderson[15] has treated the problem of continuous parallelogram plate, which may be the panels of the sweptback wing, subjected to the compressive stresses. For the problem of a parallelogram plate clamped along all edges and subjected to uniform edge stresses, Guest[16] has given the solution using Lagrangian multiplier and Wittrick[17] using Rayleigh-Ritz method. However, it seems that any report has not yet been found for the thermal deformation of a parallelogram plate.

Here one surface of the parallelogram plate with all edges clamped was heated by the infrared radiant heating apparatus and the behavior of its thermal deformation was observed. At the same time the numerical analysis was carried out on the basis of the measured temperature or strains. The dis-

* Published on the Journal of the Japan Society for Aeronautical and Space Science, Vol. 16, No. 176, (1968) (in Japanese)
** Department oi Aeronautical Engineering, College of Engineering.
*** Central Research Institute of Electric Power Industry.

placements, the stress distribution, the critical temperature for buckling and its mode were obtained and compared with the experimental results.

The rigid frame was used to satisfy the boundary conditions for clamped edges, but the clamping was unsatisfactory in practice and the deformation of the frame including the effect of the temperature rise had to be considered in the theoretical analysis.

Nomenclature

ξ , η , ζ		oblique coordinates (see Fig. 1)
d		thickness of parallelogram plate
θ		angle $\xi O \eta$ (see Fig. 1)
u, v, w		components of displacement in ξ-, η- and ζ-directions in middle plane
E		Young's modulus
ν		Poisson's ratio
D		flexural rigidity of plate
$\overline{\sigma}^{11}$, $\overline{\sigma}^{22}$, $\overline{\sigma}^{12}$		contravariant components of stress tensor in oblique system in middle plane of plate
P_{ij}, Q_{ij}, R_j, K_{i0}		coefficients in Eqs. (8) and (11) term defined by temperature in Eq. (7)
h		node interval in finite-difference method
$T(\xi , \eta , \zeta)$		temperature rise at point (ξ , η , ζ)
$\overline{T}(\xi , \eta , \zeta)$	$=$	$\frac{1}{d}\int_{-\frac{d}{2}}^{\frac{d}{2}} T(\xi , \eta , \zeta)\, d\zeta$
$\widetilde{T}(\xi , \eta , \zeta)$	$=$	$\frac{1}{d^2}\int_{-\frac{d}{2}}^{\frac{d}{2}} T(\xi , \eta , \zeta)\, \zeta d\zeta$
α	$=$	coefficient of linear thermal expansion
p	$=$	distributed load
λ	$=$	$\frac{1}{D} 2dh^2 \sin^3\theta$
∇^4	$=$	$\mathrm{cosec}^4\theta \left(\frac{\partial^2}{\partial \xi^2} - 2\cos\theta \frac{\partial^2}{\partial \xi \partial \eta} + \frac{\partial^2}{\partial \eta^2} \right)^2$

Subscripts ξ and η mean the partial differentiation with respect to ξ and η, respectively.

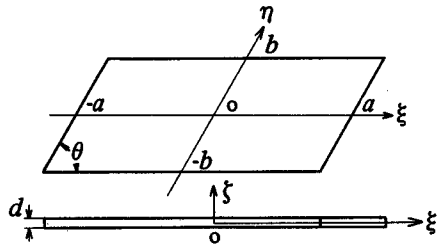

Fig. 1 Parallelogram plate

2. Experimental apparatus

i) Radiant heating unit

The heating unit used in this experiment is constructed from the strip

heater 5305-25A* (25 in. in length) which has the parabolic section to concentrate radiant heat energy and the infrared lamps of quartz-tube (2.5 KW, 480 V). Eight units were set tightly side by side, as shown in Fig. 2.

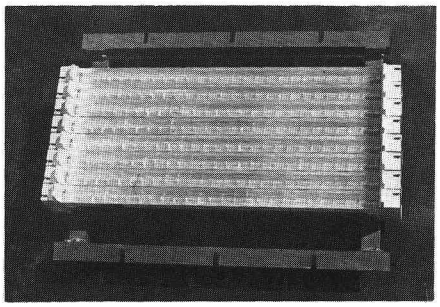

Fig. 2 Radiant heating unit

ii) Test plate and clamping frame

The test plate as shown in Fig. 3 was cut out from the polished mild steel plate. The clamping frame was machined from the steel plate of 45 mm thickness to the shape as shown in Fig. 4. As it was expected that the deformation of the frame would be caused by its temperature rise to some extent, the section as shown in Fig. 4 was taken so as to increase the rigidity and furthermore the frame was covered with heat-insulator made by glassfibre to prevent its temperature rise caused by direct heating.

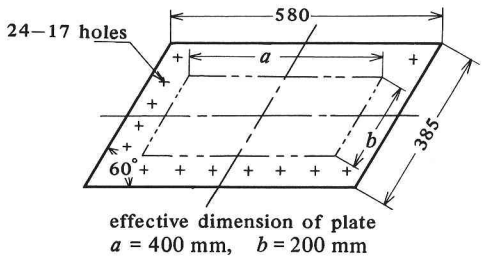

Fig. 3 Test plate

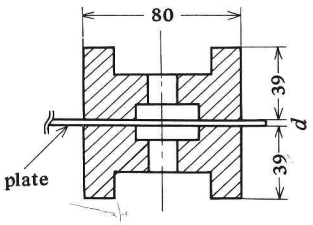

Fig. 4 Section of clamping frame

iii) Temperature, deflection and strain measurements

The temperature on the both surfaces of the plate were measured by the 0.3 mm C-C thermocouples covered with glasswool. The transient temperature variation was recorded continuously by multi-pen recorders. For the deflection measurement unbonded strain gages and differential transformers which could be connected directly to dynamic strain-meter were used. The measurement was carried out on the opposite side with the heated surface.

As shown later (Fig. 6) the buckling phenomenon was observed when the maximum temperature rise was about 120°C on the plate. In this extent of temperature rise it is possible to use the self-compensated strain gages. After mounting them on the test plate, they were subjected to a number of temperature cycles for curing and the zero point shifts of gages under stress-

* This is a Trademark of Reseach. Inc.

free condition were measured. Then, the plate was used for the experiment and the thermal strains over the plate were obtained. In this measurement the three lead wire system was adopted.

3. Experimental results

i) Temperature

For the thickness of the plate used here, e. g. 2.60 mm, the difference of temperature between the surfaces of plate was slight. Then the average value of the temperature on both surfaces was used for the theoretical analysis.

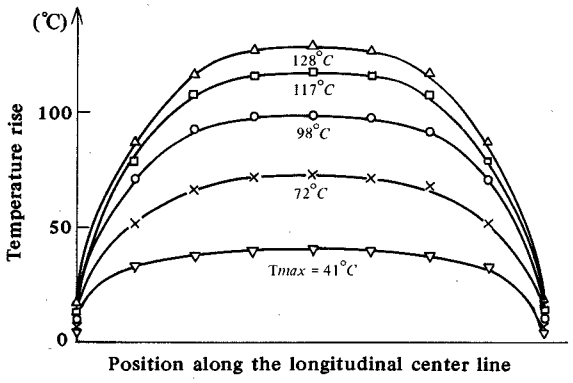

Fig.5 Example of temperature distribution

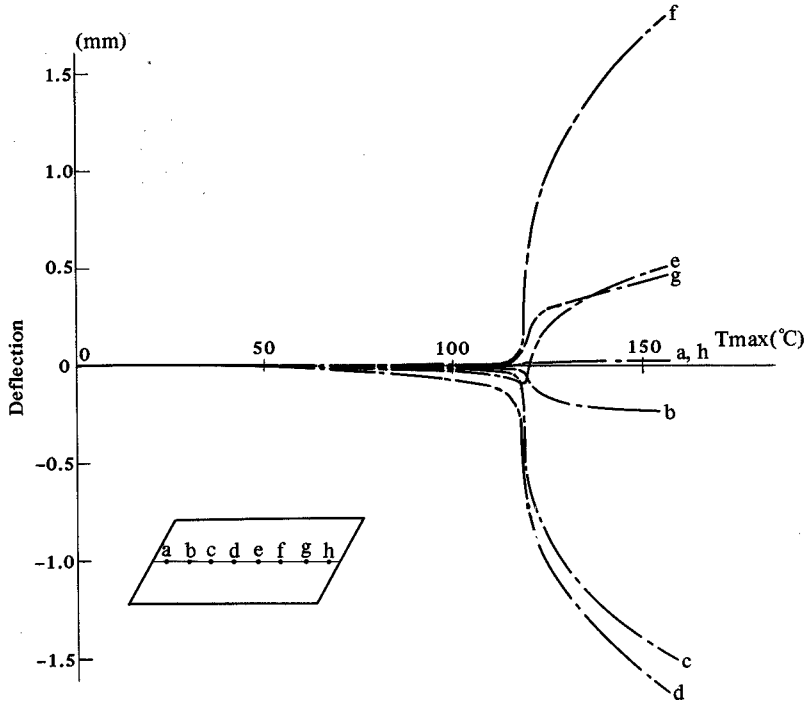

Fig.6 Variation of deflection with temperature rise of center of plate, Tmax

The temperature distribution seemed to be symmetrical with respect to the center of the plate. An example of the temperature distribution along the longitudinal center line is shown in Fig. 5.

ii) Deflection

The results of the deflection measurements are shown in Fig. 6. It is clearly observed that the buckling phenomenon occurs when the maximum temperature Tmax at the center of the plate attains to about 120°C.

iii) Strains

The stresses may be obtained from the measured strains and the results will be shown later (Fig. 12 and 13) with those obtained by the theoretical analysis.

4. Theoretical analysis

i) Fundamental equations

The displacements caused by the temperature rise of a plate must satisfy the following equations :[18,19]

$$\frac{\partial}{\partial\xi}\{u_\xi+\frac{1}{2}w_\xi^2+(\cos^2\theta+\nu\sin^2\theta)(v_\eta+\frac{1}{2}w_\eta^2)-\cos\theta(u_\eta+v_\xi+w_\xi w_\eta)\}$$
$$+\frac{\partial}{\partial\eta}\{\frac{1}{2}(1+\cos^2\theta-\nu\sin^2\theta)(u_\eta+v_\xi+w_\xi w_\eta)-\cos\theta(u_\xi+\frac{1}{2}w_\xi^2+v_\eta+\frac{1}{2}w_\eta^2)$$
$$=(1+\nu)\alpha\sin^2\theta\,(\overline{T}_\xi-\overline{T}_\eta\cos\theta) \tag{1}$$

$$\frac{\partial}{\partial\xi}\{\frac{1}{2}(1+\cos^2\theta-\nu\sin^2\theta)(u_\eta+v_\xi+w_\xi w_\eta)-\cos\theta(u_\xi+\frac{1}{2}w_\xi^2+v_\eta+\frac{1}{2}w_\eta^2)\}$$
$$+\frac{\partial}{\partial\eta}\{(\cos^2\theta+\nu\sin^2\theta)(u_\xi+\frac{1}{2}w_\xi^2)+v_\eta+\frac{1}{2}w_\eta^2-\cos\theta(u_\eta+v_\xi+w_\xi w_\eta)\}$$
$$=(1+\nu)\alpha\sin^2\theta\,(\overline{T}_\eta-\overline{T}_\xi\cos\theta) \tag{2}$$

$$\frac{\partial}{\partial\xi}\Big[w_\xi\{u_\xi+\frac{1}{2}w_\xi^2+(\cos^2\theta+\nu\sin^2\theta)(v_\eta+\frac{1}{2}w_\eta^2)-\cos\theta(u_\eta+v_\xi+w_\xi w_\eta)\}$$
$$+w_\eta\{\frac{1}{2}(1+\cos^2\theta-\nu\sin\theta)(u_\eta+v_\xi+w_\xi w_\eta)-\cos\theta\,(u_\xi+\frac{1}{2}w_\xi^2+v_\eta+\frac{1}{2}w_\eta^2)\}\Big]$$
$$+\frac{\partial}{\partial\eta}\Big[w_\eta\{(\cos^2\theta+\nu\sin^2\theta)(u_\xi+\frac{1}{2}w_\xi^2)+v_\eta+\frac{1}{2}w_\eta^2-\cos\theta(u_\eta+v_\xi+w_\xi w_\eta)\}$$
$$+w_\xi\{\frac{1}{2}(1+\cos^2\theta-\nu\sin^2\theta)(u_\eta+v_\xi+w_\xi w_\eta)-\cos\theta(u_\xi+\frac{1}{2}w_\xi^2+v_\eta+\frac{1}{2}w_\eta^2)\}\Big]$$
$$-\frac{d^2}{12}\{w_{\xi\xi\xi\xi}-4\cos\theta\,w_{\xi\xi\xi\eta}+2(1+2\cos^2\theta)w_{\xi\xi\eta\eta}-4\cos\theta\,w_{\xi\eta\eta\eta}+w_{\eta\eta\eta\eta}\}$$
$$=(1+\nu)\alpha\sin^2\theta\Big[d(\widetilde{T}_{\xi\xi}+\widetilde{T}_{\eta\eta}-2\cos\theta\,\widetilde{T}_{\xi\eta})$$
$$+\frac{\partial}{\partial\xi}\{\overline{T}(w_\xi-w_\eta\cos\theta)\}+\frac{\partial}{\partial\eta}\{\overline{T}(w_\eta-w_\xi\cos\theta)\}\Big]$$
$$-\frac{1-\nu^2}{Ed}\sin^4\theta\,p \tag{3}$$

As it is very complicated to solve these equations directly, they are linearized.

First, the covariant components of displacement u and v in the middle plane must satisfy

$$u_{\xi\xi} - 2\cos\theta u_{\xi\eta} + \frac{1}{2}(1+\cos^2\theta - \nu\sin^2\theta)u_{\eta\eta} - \cos\theta v_{\xi\xi} - \cos\theta v_{\eta\eta}$$
$$+ \frac{1}{2}(1+3\cos^2\theta + \nu\sin^2\theta)v_{\xi\eta} = \alpha(1+\nu)\sin^2\theta(\bar{T}_\xi - \bar{T}_\eta\cos\theta) \tag{4}$$

$$-\cos\theta u_{\xi\xi} + \frac{1}{2}(1+3\cos^2\theta + \nu\sin^2\theta)u_{\xi\eta} - \cos\theta u_{\eta\eta} + \frac{1}{2}(1+\cos^2\theta - \nu\sin^2\theta)v_{\xi\xi}$$
$$- 2\cos\theta v_{\xi\eta} + v_{\eta\eta} = \alpha(1+\nu)\sin^2\theta(\bar{T}_\eta - \bar{T}_\xi\cos\theta) \tag{5}$$

and the deflection w must satisfy

$$D\nabla^4 w = d\,\mathrm{cosec}\,\theta(\bar{\sigma}^{11}w_{\xi\xi} + 2\bar{\sigma}^{12}w_{\xi\eta} + \bar{\sigma}^{22}w_{\eta\eta}) \tag{6}$$

Transforming these equations to the finite-difference equations for the nodal points shown in Fig. 7, the following relations are obtained:

$$\sum_{j=0}^{8}(P_{ij}u_j + Q_{ij}v_j) = K_{i0}\,(i = 1,2) \tag{7}$$

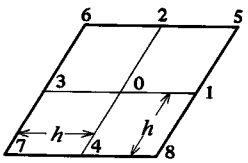

Fig. 7 Representative nodal point arrangement for Eq. (7)

where

$$\left.\begin{aligned}
&P_{10} = Q_{20} = -(3 + \cos^2\theta - \nu\sin^2\theta)\\
&P_{12} = P_{14} = Q_{21} = Q_{23} = \frac{1}{2}(1 + \cos^2\theta - \nu\sin^2\theta)\\
&P_{11} = P_{13} = Q_{22} = Q_{24} = 1\\
&-P_{15} = P_{16} = -P_{17} = P_{18} = -Q_{25} = Q_{26} = -Q_{27} = Q_{28} = \frac{1}{2}\cos\theta\\
&P_{20} = Q_{10} = 4\cos\theta\\
&P_{21} = P_{22} = P_{23} = P_{24} = Q_{11} = Q_{12} = Q_{13} = Q_{14} = -\cos\theta\\
&P_{25} = -P_{26} = P_{27} = -P_{28} = Q_{15} = -Q_{16} = Q_{17} = -Q_{18}\\
&\qquad = \frac{1}{8}(1 + 3\cos^2\theta + \nu\sin^2\theta)
\end{aligned}\right\} \tag{8}$$

$$K_{10} = \frac{1}{2}\alpha h(1+\nu)\sin^2\theta\,\{T_1 - T_3 - \cos\theta(T_2 - T_4)\}$$
$$K_{20} = \frac{1}{2}\alpha h(1+\nu)\sin^2\theta\,\{T_2 - T_4 - \cos\theta(T_1 - T_3)\}$$

Therefore two difference equations (7) are obtained for each nodal point of network shown in Fig. 7. If the temperature distribution is symmetrical with respect to the center of the parallelogram plate, the displacement vector has the same symmetrical character with respect to the center and there is no displacement at the center. Then, we have only to solve the equations (7) for nodal points 1, 2, ... , 10 in Fig. 8. Obtaining the covariant components of

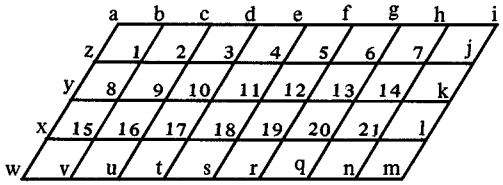

Fig. 8 Nodal point arrangement on plate

the displacement, the contravariant components of the stress tensor are calculated numerically from the following relation

$$\begin{bmatrix} \bar{\sigma}^{11} \\ \bar{\sigma}^{22} \\ \bar{\sigma}^{12} \end{bmatrix} = \frac{E\operatorname{cosec}^3\theta}{1-\nu^2} \begin{bmatrix} 1 & \cos^2\theta + \nu\sin^2\theta & -\cos\theta \\ \cos^2\theta + \nu\sin^2\theta & 1 & -\cos\theta \\ -\cos\theta & -\cos\theta & \frac{1}{2}(1+\cos^2\theta - \nu\sin^2\theta) \end{bmatrix}$$

$$\times \begin{bmatrix} u_\xi \\ v_\eta \\ u_\eta + v_\xi \end{bmatrix} - \frac{E\alpha\bar{T}}{1-\nu^2} \begin{bmatrix} \operatorname{cosec}\theta \\ \operatorname{cosec}\theta \\ -\cot\theta \end{bmatrix} \tag{9}$$

Substituting these stresses into Eq. (6) and transforming the equation to the finite-difference equation for the nodal points shown in Fig. 9. the following relations are obtained :

$$\sum_{j=0}^{20} R_j w_j = 0 \tag{10}$$

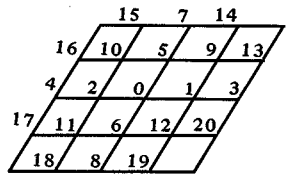

Fig. 9 Representative nodal point arrangement for Eq. (10)

where

$$\left.\begin{aligned} R_0 &= 40\ (1+\tfrac{4}{5}\cos^2\theta) + 2\lambda(\bar{\sigma}^{11}+\bar{\sigma}^{22}) \\ R_1 &= R_2 = -\{16\,(1+\cos^2\theta) + \lambda\bar{\sigma}^{11}\} \\ R_3 &= R_4 = R_7 = R_8 = 2 \\ R_5 &= R_6 = -\{16\,(1+\cos^2\theta) - \lambda\bar{\sigma}^{22}\} \end{aligned}\right\} \tag{11}$$

$$R_9 = \underline{R}_{11} = 4\,(\,1 + 2\cos\theta + 2\cos^2\theta\,) - \frac{1}{2}\lambda\bar{\sigma}_{12}$$
$$R_{10} = R_{12} = 4\,(\,1 - 2\cos\theta + 2\cos^2\theta\,) + \frac{1}{2}\lambda\bar{\sigma}_{12}$$
$$-R_{13} = -R_{14} = R_{15} = R_{16} = -R_{17} = -R_{18} = R_{19} = R_{20} = 2\cos\theta$$
$$\lambda = \frac{1}{D}2dh^2\sin^3\theta$$

Considering the case of all edges clamped, the relation

$$w_o = w_i \tag{12}$$

is available for the inner point i and the outer point o near the boundary as shown in Fig. 10. Therefore, adding the outer nodal points outside the domain

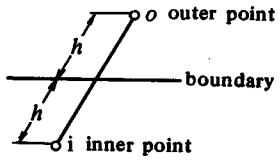

Fig. 10 Nodal points adjoining boundary

of Fig. 8 and eliminating w of these outer points using Eq. (12), the simultaneous linear equations about w at the inner nodal points are obtained. When the determinant of the coefficients of the above equations becomes zero, the

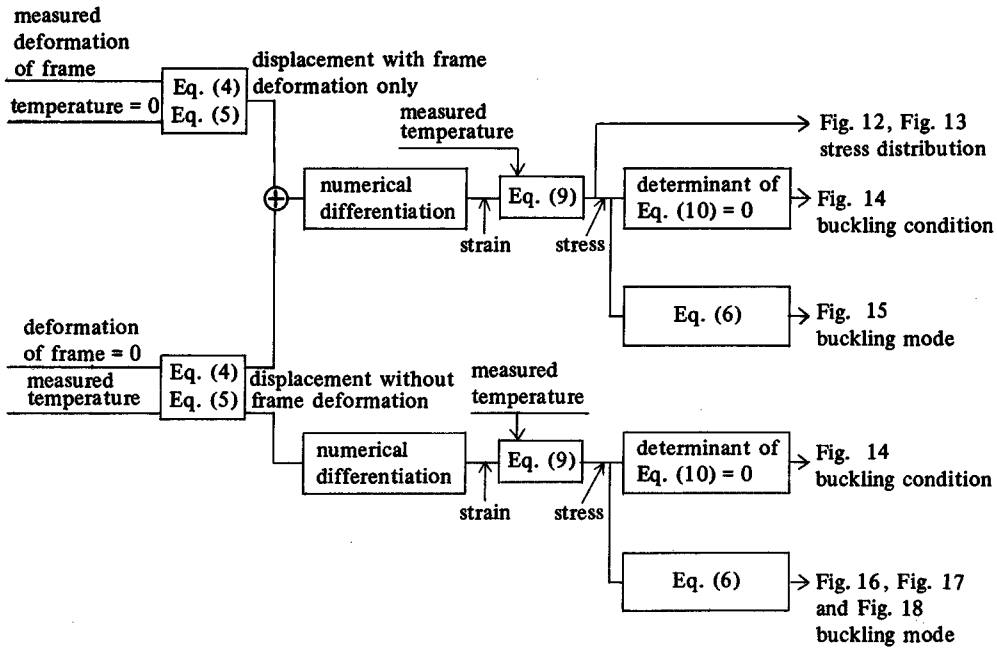

Fig. 11 Procedure diagram of analysis

thermal buckling will occur. Then, drawing the curve by taking the temperature rise at the central point of the plate for the abscissa and the value of the above-mentioned determinant for the ordinate, the critical temperature for the thermal buckling will be obtained at the point where the curve crosses the abscissa.

ii) Numerical calculation

Covariant components (u, v) of the displacement at each nodal point are obtained by substituting the temperature rise obtained by the actual measurement (section 3 (i)) into Eq. (8) and solving the difference equations (7). For the arrangement of the nodal points shown in Fig. 8, these become the simultaneous linear equations with 20 unknowns and the calculation was carried out by the digital computer for several temperature distribution after the beginning of heating.

On the above calculation, it was first assumed that the plate was clamped rigidly and there was no deflection of the clamping frame, but the frame slightly deformed on heating. Therefore, Eqs. (7) were solved under the measured boundary displacements (u, v) and zero temperature rise. These results were superposed on the former solution to take the effect of deformation of the frame into consideration. The procedure of these analysis is shown in Fig. 11.

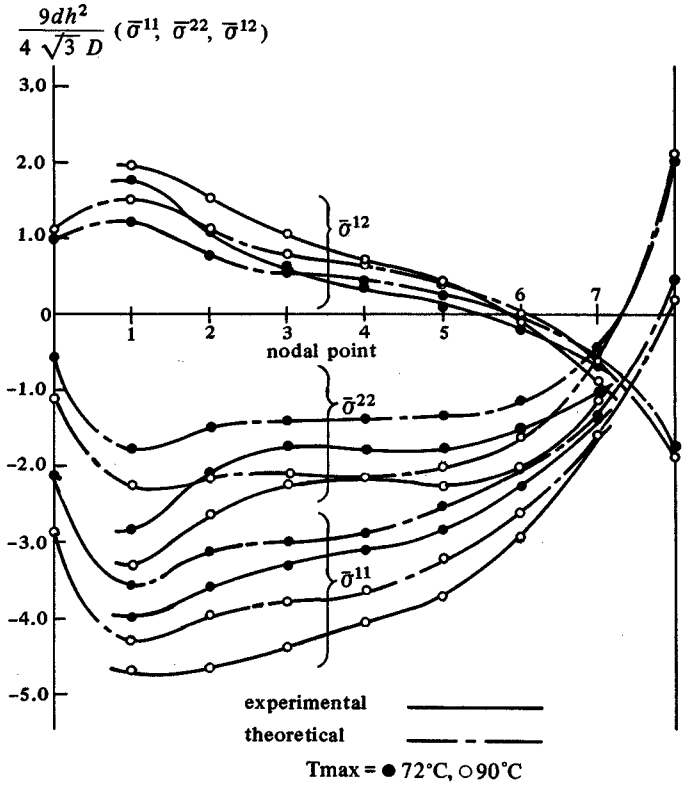

Fig. 12 Comparison of theoretical and experimental stress distribution

Substituting the measured temperature rise and the displacements calculated as above into Eq. (9), the plane stresses may be determined. These results and those obtained by strain measurements are shown in Figs. 12 and 13. They seems to show good agreement in spite of the difficulty of strain measurement at high temperature. Substituting these stresses into Eqs. (10), we are able to calculate the determinant of the coefficient of w's. The value of determinant is shown in Fig. 14 for two cases with and without the deformation of the frame. It is shown in Fig. 14 that the thermal buckling occurs rather early in the case with no deformation of the frame. Figs. 6 and 14 show that the temperature $T_{\max,cr}$ obtained by the theoretical analysis with consideration for the deformation of the frame, agrees approximately with the temperature at which the measured deflection begins to increase. Fig. 15 shows the correlation between theoretical and experimental results of the buckling mode for the case with the deformation of the frame. Both results are thought to conform to each other on the whole considering that a few error are unavoidable from the influence of initial deflection of the plate,etc. On the other hand Fig. 16 through Fig. 18 show the modes analyzed for three buckling temperatures, at which the curve of Fig. 14, for the frame without deformation, crosses the abscissa.

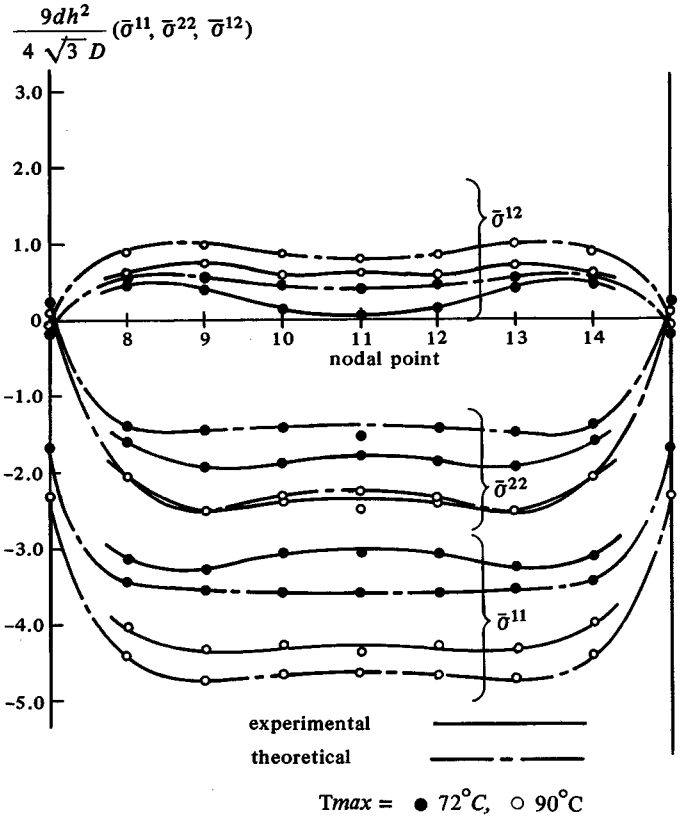

Fig. 13 Comparison of theoretical and experimental stress distribution

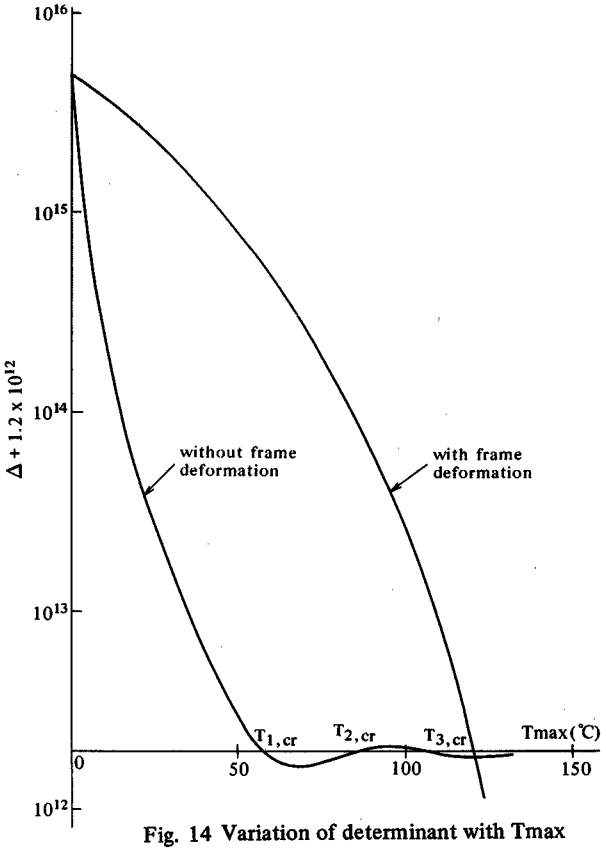

Fig. 14 Variation of determinant with Tmax

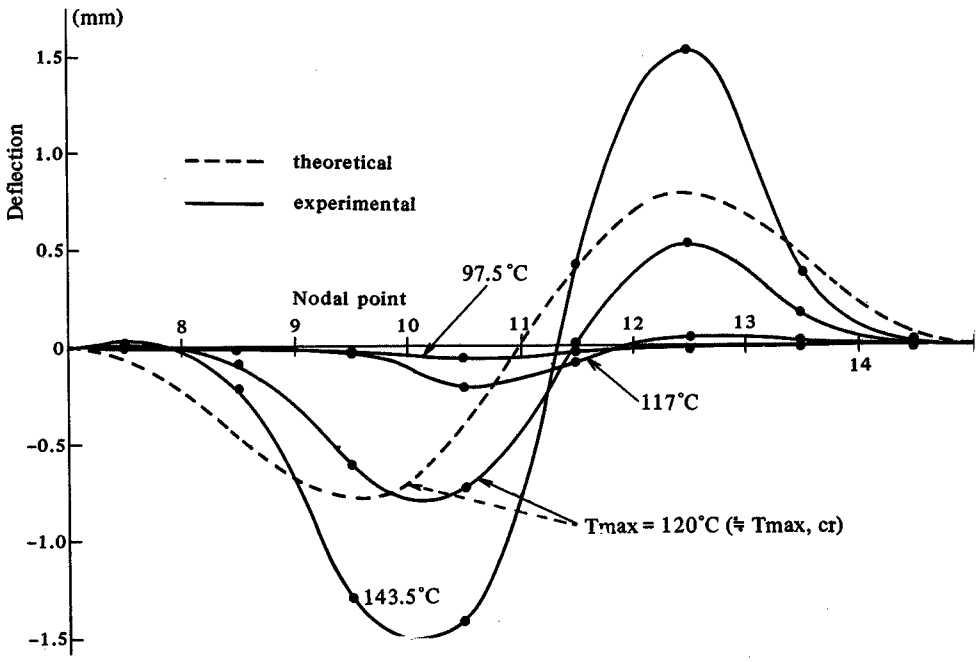

Fig. 15 Comparison of buckling mode

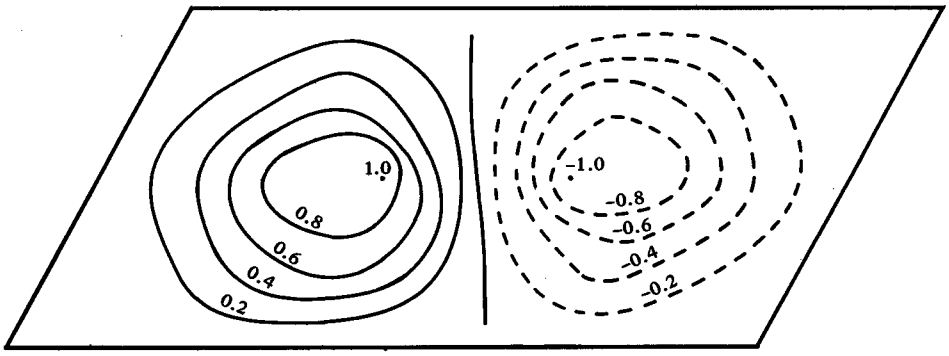

Fig. 16 Buckling mode (deflection surface) for T1, cr (see Fig. 14)

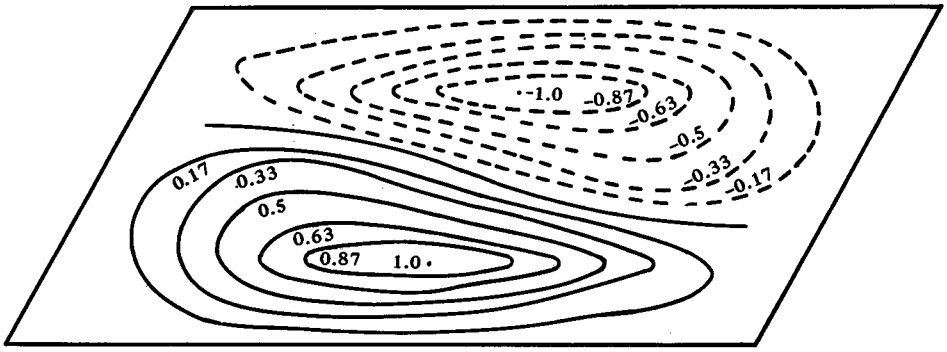

Fig. 17 Buckling mode (deflection surface) for T2, cr (see Fig. 14)

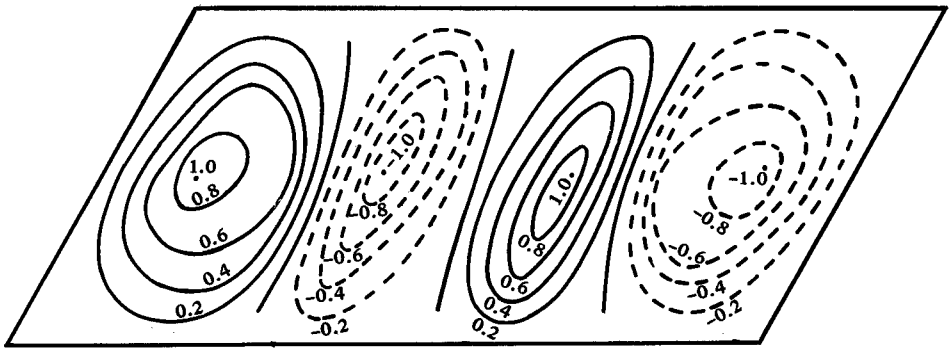

Fig. 18 Buckling mode (deflection surface) for T3, cr (see Fig. 14)

5. Conclusion

This work treated experimentally and theoretically the thermal deformation of the parallelogram plate clamped along all edges under the uniform radiant heating

In the experiment the parallelogram plate was heated on one surface with the infrared radiant heating apparatus and the temperature rise, the deflection

and the strain distribution on the plate were obtained. The buckling phenomenon was clearly observed and the critical temperature rise for buckling at the center of the plate was about 120° C. In this range of temperature rise, it was possible to use the self tempeature-compensated strain gages and thermal strains on the plate were measured. Next the fundamental differential equations of displacements in nonlinear form were derived. As it was very complicated to solve these equations directly, they were linearized and using such equations, the deflection and stress distribution caused by the measured temperature distribution were obtained. The comparison of the theoretical stress distribution with the experimental ones showed rather good agreement. Furthermore, the critical temperature for buckling and buckling modes were obtained and compared with the experimental results.

Acknowledgements

The work reported herein originated with the scientific research for the testing sponsored by the Ministry of Education from 1966 to 1967. The authors would like to express their appreciation to Prof. M. Uemura of the Institute of Aeronautical and Space Science, University of Tokyo, for offering some apparatus for this work. The authors also gratefully acknowledge the assistance of Mr. Y. Yada and Mrs. F. Watanabe for the experiment and the numerical calculation and of Miss F. Konaka for manuscripts.

6. References

1) E.W. Parkes , Aircraft Engng., XXV, 298, 373 (1953).
2) G. Isackson, J. Aero. Sci., **24**, 8, 611 (1957).
3) H. Tramposch , J. Aero. Sci., **29**, 6, 719 (1962).
4) N.J. Hoff , J. Aero. Sci., **23**, 11, 1019 (1956).
5) A. van der Neut, High temperature effects in aircraft structures, Pergamon Press, New York (1958).
6) M. Uemura and M. Sunakawa , Proc. the 10th Japan Natl. Congr. Appl. Mech., 55 (1960).
7) M. Sunakawa and M. Uemura , Trans. Japan Soc. Mech. Engng., **27**, 179, 1074 (1961).
8) M. Sunakawa and M. Uemura , Aero. Res. Inst., Univ. of Tokyo., Rep. 359, (1960).
9) M. Sunakawa , J. Japan Soc. Aero. Space Sci., **9**, 85, 37 (1961).
10) M. Uemura, M. Sunakawa and M. Fuyuki , J. Japan Soc. Aero Space Sci., **10**, 98, 79 (1962).
11) M. Sunakawa, T. Watanabe, K. Inoue and S. Abe , J. Japan Soc. Aero. space Sci., **15**, 157,39 (1967).
12) K. Miura , Aero. Res. Inst., Univ. of Tokyo, Rep. 353 (1960).
13) M. Uemura , Aero. Res. Inst., Univ. of Tokyo, Rep. 352 (1960).
14) Y. Sugiyama, T. Sekiya and S. Sumi , Bull. Univ. Osaka Pref., **A 16**, 1, 29 (1967).
15) R.A. Anderson , NACA TN 2392 (1951).
16) J. Guest , Aero. Res. Lab., Rep. 172 (Australia), (1951).
17) W.H. Wittrick , Aero. Quart., **4**, 151 (1953).
18) W.S. Hemp , Aero. Quart., **7**, 184 (1956).
19) T. Katayama, E. Matsumoto and T. Sekiya , Bull. Univ. Osaka Pref., **A 16**. 2 (1967).
20) Y. Yoshimura , J. Japan Soc. Aero. Space Sci., 1, 3, 127 (1953).
21) L.S.D. Morley , Skew plates and structures, Pergamon Press, New York (1963).